Nucleation of diamond from liquid carbon under extreme pressures: Atomistic simulation

A. Sorkin,* Joan Adler, and R. Kalish
Physics Department, Technion, Israel Institute of Technology, Haifa, 32000, Israel
(Received 27 April 2006; published 31 August 2006)

The stable solid form of carbon is graphite; diamond is thermodynamically unstable at atmospheric pressure. High pressure and high temperature must be applied to enable diamond crystal growth. Cubic diamond grows when hydrostatic pressure is applied, whereas hexagonal diamond (which is another form of sp^3-hybridized carbon) has been reported to grow when uniaxial pressure is applied. In the present study, we simulate the precipitation and growth of diamond clusters inside an amorphous carbon network by rapid quenching of the compressed liquid phase, followed by volume expansion. The simulations are carried out under both hydrostatic (in all three directions) and uniaxial pressure, exposing the samples to different initial pressures (densities) as well as to different cooling rates. At fast cooling rates (500–1000 K/ps) and high densities (3.7–3.9 g/cc), large diamond crystallites (containing up to 120 atoms) are formed. We find that the probability of precipitation of diamond crystallites increases with density and with cooling rate. Uniaxial compression of the samples does not lead to nucleation of the hexagonal form of diamond; all uniaxially compressed ordered sp^3 clusters were identified to be cubic diamond, with random orientation relative to the compression direction. At slower cooling rates (200–500 K/ps), some samples transform to graphite with an interplanar distance smaller than that of perfect graphite. Graphite formed under hydrostatic pressure has planes with random oreintation, whereas the planes of graphite formed under uniaxial pressure were oriented in parallel with the direction of compression.

DOI: 10.1103/PhysRevB.74.064115 PACS number(s): 62.50.+p, 81.05.Uw, 61.43.Bn

I. INTRODUCTION

Carbon can form a wide variety of solid structures due to its different bonding configurations. When sp^2 bonds are formed, the resulting bulk carbonaceous material is graphite, whereas sp^3 bonding results in the formation of cubic or hexagonal diamond (c-D and h-D, respectively). These two allotropes of carbon, graphite, and diamond, exhibit vastly different physical and chemical properties. Diamond, being the most tightly bonded solid crystal in nature, is extremely hard, has outstanding thermal and chemical properties, and is a wide band gap semiconductor. In contrast, graphite is a soft layered material with semimetallic electrical properties. Even though the ground-state energies of diamond and graphite are quite similar (with graphite being slightly more stable then diamond), a high potential barrier separates these two allotropes of carbon. Much effort, both experimental and theoretical, has been devoted to the question of how graphite can be transformed into diamond. According to the phase diagram of carbon,[1] high pressures and high temperatures are required to cause this transformation, i.e., to overcome the potential energy barrier between graphite and diamond.

It is interesting that sp^3-bonded carbon was found to exist not only as cubic crystals but also as hexagonal crystals (Londsdaleite). These were first found in meteorites, then later grown in the laboratory.[2] In contrast to the high-pressure high-temperature (HPHT) cubic diamond growth achieved under hydrostatic pressure, hexagonal diamond was observed to grow when uniaxial pressure was applied to liquid carbon during its solidification. Cubic and hexagonal diamond, both being composed of sp^3-bonded carbon atoms, have a rather similar structure, differing only in the stacking order of the sp^3-bonded carbon layers. The angles between C-C bonds is 109°, and the interatomic distance is 1.54 Å for both these forms of crystalline diamond. The difference between c-D and h-D is only apparent when looking at the longer-range structural properties of C atoms in the crystals. Figures 1 and 2 show the structures of ideal c-D and h-D crystals and their radial distribution functions. The similarity between these should be noted.

A. Experimental background

The technical problem of how to overcome the barrier that separates sp^2-hybridized graphite from sp^3-hybridized diamond was first solved by the General Electric Research Laboratory scientists in 1955, who succeeded in extending the range of laboratory achievable pressures to about 7 GPa (~70 000 atm) with temperatures within the pressurized volume of about 6000 K. Under these extreme conditions, Bundy and co-workers showed that graphite can be artificially converted to diamond in the presence of catalysts.[1,3,4] It was later shown that diamond can be synthesized from graphite by direct conversion under high pressure and high temperature (HPHT) even without using catalysts (above 10 GPa and 2000 °C).[5–8]

Another technique of HPHT synthesis of diamond from carbonaceous materials makes use of the short time compression and high temperatures achievable during detonation.[9,10] In 1961, graphite was converted directly to diamond by this technique using the shock compression and high temperatures obtained during explosion that create, for a few microseconds, a pressure of about 35 GPa. Various types of carbonaceous precursors can be used in this detonation process, including graphite, carbon black, fullerenes, and organic substances, but among these, graphite is the most widely used. The diamonds produced by this method were found to be largely influenced by the structure and size of precursors as

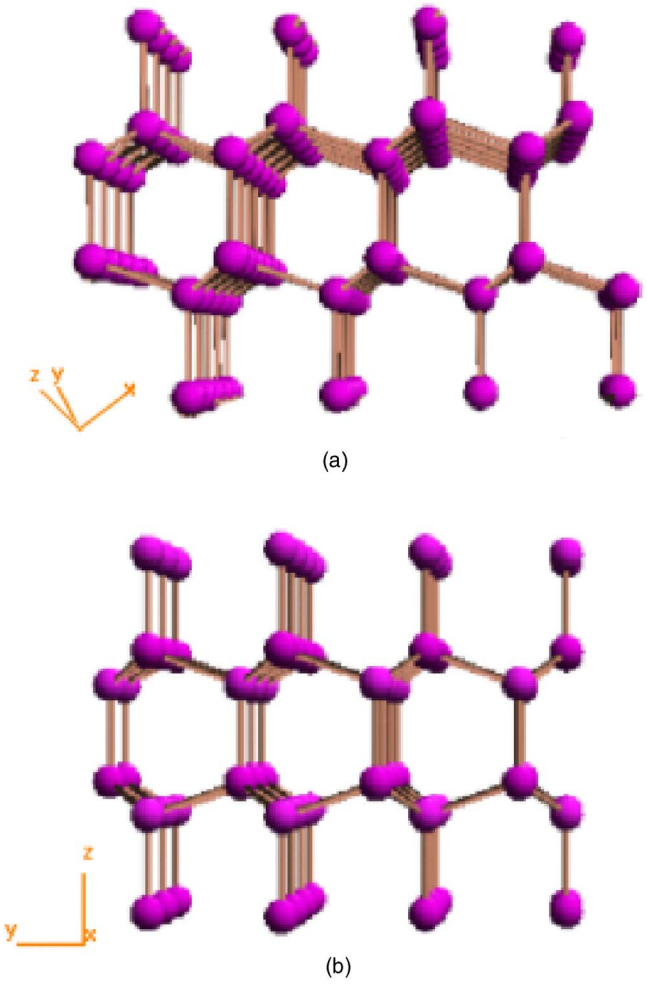

FIG. 1. (Color online) Structures of (a) perfect cubic diamond and (b) perfect hexagonal diamond. These viewpoints show the similarity between these structures. Differences can be seen by careful observation of the hexagons: at these angles, each hexagon appears to have two short and four long bonds. In cubic diamond, the short bonds are on opposite side of the hexagons separated by two long bonds, whereas in hexagonal diamond either one or three long bonds separate these two short bonds. We note that, in fact, the hexagons are not in a plane, and all bonds are of the same length. The apparent lengths of the bonds are due to the viewing angle.

well as by the physical process employed. It was shown that an increase in pressure during the explosion leads to a higher diamond content in the detonation soot.[11,12]

After explosion, the system passes through the pressure-temperature region in the carbon phase diagram where the graphitic phase is preferable. To enhance the growth of diamond relative to that of graphite, the time spent in this region must be minimized. Hence, the role that the cooling rate after detonation plays in the final formation of the solid carbon structure is crucial. Titov *et al.*[13] have shown that an increase of the cooling rate led to preferred precipitation of diamond due to the reduction of the time the system spends in the undesirable region of the phase diagram.

Diamond crystallites can also form from dense clusters of carbon atoms during "biased enhanced nucleation" [which is a way to create sub-nano-sized diamond nucleation centers

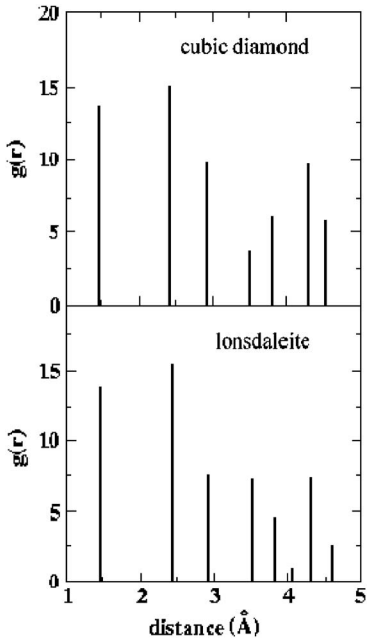

FIG. 2. Radial distribution, $g(r)$, of perfect cubic diamond (top) compared to that of perfect lonsdaleite (bottom). The radial distribution functions were calculated for samples containing 64 atoms.

for subsequent chemical vapor deposition (CVD) diamond growth].[14,15] In this method, ions from the growth plasma, which contains H+, C+, and other positively charged C-H radicals, are accelerated by several hundred volts toward a negatively biased substrate. The bombardment of these ions leads to the subplantation[15] of carbon and hydrogen ions into subsurface regions. Lifshitz and co-workers proposed that once a high concentration of sp^3-bonded amorphous C clusters is reached in this way, some clusters can crystallize to form perfect diamond crystallites that can be several nanometers in size. It was shown by high-resolution TEM (transmission electron microscopy) that prior to the formation of the diamond, growth of graphitic planes, perpendicular to the substrate surface, takes place.[16] These can be densified by subsequent ion bombardment and can eventually form diamond crystallites. The physics of this process is related to the stopping process of implanted ions in matter. It is well known that during the slowing down of ions, many atoms of the stopping medium are displaced, resulting in the formation of a "thermal spike." This is a few nanometers in size and lasts for about a picosecond, i.e., during this time a small region of the material experiences very high temperatures and local high pressures. Hence, the biased enhanced nucleation process thermal spikes within a dense C cluster can drive the system into the HPHT region in the C phase diagram in which diamond formation is favored, resulting in the formation of tiny diamond clusters.

B. Computational background

Several first-principles computer simulations have been carried out to model the conversion of graphite or amorphous carbon to diamond under different conditions.[17–20] Scandolo *et al.*[18] found that under hydrostatic pressure (i.e., identical

TABLE I. Fraction of four-, three-, and twofold coordinated atoms in the entire amorphous carbon sample subjected to the cooling rate of 500 K/ps. The number of cases (out of five), where a diamond cluster containing more than 20 atoms was generated, are given in the last column. The numbers in brackets are the numbers of atoms in each such cluster.

Density (g/cc)	Fourfold (%)	Threefold (%)	Twofold (%)	Number of diamond clusters
3.3	52±4	44±4	4±4	0
3.5	72±3	24±5	4±2	0
3.7	83±6	17±3	0	2 (22, 31)
3.9	88±2	11±2	1±1	4 (26, 45, 90, 120)
4.1	95±3	5±3	0	3 (21, 21, 25)

pressure applied in all directions) of 30 GPa, graphite transforms to orthorhombic graphite, followed by the collapse of the graphitic planes to form both cubic and hexagonal forms of carbon. Calculations by Tateyama *et al.*[19] showed that the activation barrier to convert graphite into cubic diamond is lower than that to form hexagonal diamond. According to these calculations, hexagonal diamond can be obtained only when the collective sliding of the graphitic planes is prohibited.

Yao *et al.*[21] have simulated the bias enhanced nucleation (BEN) of diamond, which is the initial stage of CVD diamond growth, by nonorthogonal tight-binding molecular dynamics computations. They found that a defective diamond cluster, containing 41 carbon atoms formed within the region where high concentrations of carbon atoms are present in an amorphous structure. According to their explanations, the diamond crystallite forms in an amorphous carbon network generated during the subplantation process, by quenching the random liquid carbon structure at a density of 3.5 g/cc.

Wang *et al.*[22] have investigated, by performing tight-binding simulations, the structures of amorphous carbon over a wide range of densities (from 2.2 to 4.4 g/cc) generated by rapid quenching of liquid carbon phase. As will be shown below, the conditions of their simulations are very similar to those reported here. However, in contrast to our findings and in spite of the fact that the percentage of sp^3-coordinated atoms was found by Wang *et al.* increase with density reaching 89% at a density of 4.4 g/cc, the authors could not identify any ordered sp^3 clusters in their samples. We consistently find diamond crystallites formed within the amorphous carbon network.

In this paper, we describe the results of tight-binding computations that simulate the fast quenching of a compressed liquid carbon sample. This procedure is similar to that occurring during the bias-enhanced nucleation process. We can artificially generate very high pressures by changing the material density (shortening the bond lengths) and very high temperatures by imparting high kinetic energies to the atoms in the simulated sample. The times available to perform molecular-dynamics (MD) computations (a few picoseconds) and the sample sizes (containing a few hundred atoms) are similar to those of the thermal spike. The densities at which

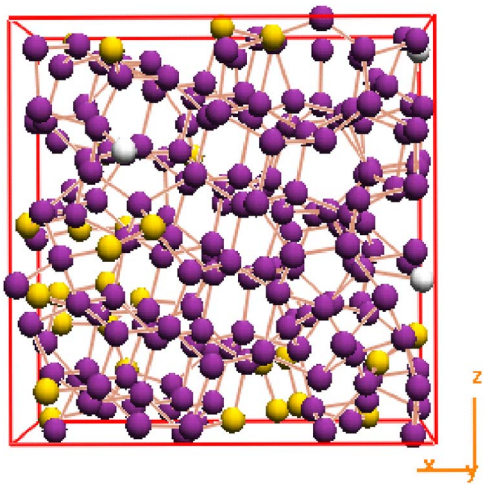

FIG. 3. (Color online) The sample of amorphous carbon with the diamond cluster inside generated at 3.9 g/cc. Black (purple online) balls are sp^3-coordinated atoms, gray (yellow online) balls are sp^2-coordinated atoms, and white balls are sp-coordinated atoms.

our simulations were carried out (3.5–4.1 g/cc) can reasonably be locally attained within the thermal spike.

We note that our samples are, of course, smaller than those in the laboratory. The latter are almost "infinite" and much larger than can be simulated today. There is extensive literature on the effect of finite size in phase transitions, where, because these are cooperative effects dependent on correlation length, there is a beautiful scaling theory describing the approach to infinite size. A similar but less dramatic situation for finite samples of diamond interface was described by Rosenblum *et al.*,[23] who showed that sample size strongly influenced results for lattice mismatch at a diamond-substrate interface. More recently in an earlier paper of ours,[24] the effect of system size on temperature was discussed. We observed that temperature, which in the simulations is essentially kinetic energy, depends on and scales with the system size.

The method we use, tight-binding molecular dynamics,[22] describes different carbon polytypes.[22,24,25] It has been shown that the energies, vibrational and elastic properties for differently coordinated crystalline structures (diamond, graphite, linear chain) calculated with the tight-binding potential are in very good agreement with first-principles calculations and experimental data.[26] Simulations of liquid and amorphous carbon indicate that the potential is reliable for describing low-coordinated carbon systems over a wide range of bonding environments. The description of the more than fourfold-coordinated structures, such as simple cubic, β-tin, or bcc structures, is only qualitative with this potential; however, since they do not exist in nature, this is not relevant here. The reliability of this potential for fullerene and single-wall carbon nanotube calculations was also tested successfully by comparison to first-principles results.[26]

We study the dependence of the final nanocrystallite phases formed as a function of the magnitude and direction of the pressure (both hydrostatic and uniaxial) and cooling rate applied. We find that, both under hydrostatic and uniaxial pressure, cubic diamond clusters are formed inside

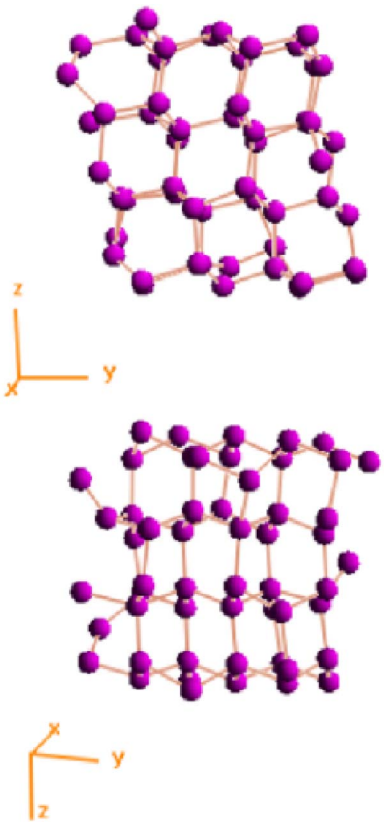

FIG. 4. (Color online) The damaged diamond cluster generated at a density of 3.9 g/cc from two different view points.

the generated amorphous network. The probability of precipitation of diamond clusters increases with density and cooling rate. The orientations of the diamond clusters were found to be random. No hexagonal diamond clusters were identified, even when uniaxial pressure was applied to the samples during cooling from the liquid. For slower cooling rates, graphitic planes were found.

II. DETAILS OF THE SIMULATIONS

Our calculations were carried out at constant volume (density). Periodic boundary conditions were applied to the samples in all three directions. In order to describe the interactions between carbon atoms, we used the tight-binding model[22] of the OXON package.[27] The electron wave functions were expanded in terms of a basis set of valence electron wave functions, controlling the attractive part of the potential, while the repulsive one was treated empirically. The Γ-point Brillouin zone sampling was used for the electronic calculations, and the MD step was 0.5×10^{-15} s. Visualization with the ATOMIC VIZUALIZATION package (AViz)[28] was applied to identify diamond clusters.

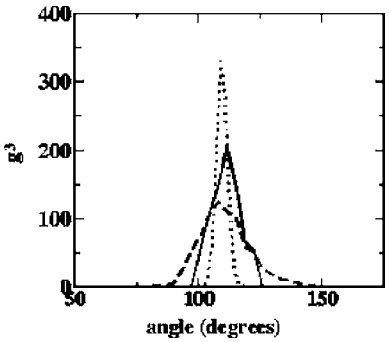

FIG. 5. Angular distribution function, $g3$, of the diamond cluster generated at 3.9 g/cc (solid line) compared to the angular distribution functions of pure diamond (dotted line) and of amorphous carbon (dashed line).

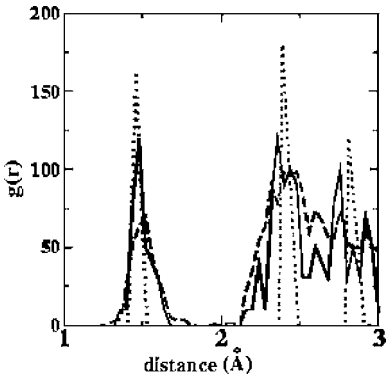

FIG. 6. Radial distribution function of the diamond cluster generated at 3.9 g/cc (solid line) compared to the radial distribution functions of a pure diamond crystal (dotted line) and of amorphous carbon (dashed line).

In order to generate amorphous carbon networks with different densities, a pure diamond sample with a density of 3.3 g/cc containing 216 atoms ($3\times3\times3$ diamond unit cells) was melted at a temperature of 8000 K during 5, 10, 15, 20, and 25 ps. Then each of the five liquid configurations were isotropically compressed by changing the volume of the unit cell to 3.3, 3.5, 3.7, 3.9, and 4.1 g/cc followed by a rapid cooling to 300 K with cooling rates of 500 K/ps, 25 simulations in all. Pressures at 8000 K for the densities of 3.3, 3.5, 3.7, 3.9, and 4.1 g/cc correspond to 60, 80, 110, 140, and 250 GPa respectively. In order to simulate an expansion, samples at 3.7, 3.9, and 4.1 were then homogeneously expanded to reduce the density to 3.5 g/cc. Then the samples were "annealed" by repeatedly heating to 1000 K and then cooling to 300 K during 10 ps. As a result of this repeated annealing cycle, only a few atoms slightly changed their position or their hybridization (for example, in the sample of 3.9 g/cc, the percentage of the sp^3-coordinated atoms changed from 88 to 86 %). The diamond clusters remained stable.

TABLE II. Band gap of the best unrelaxed diamond cluster at each density compared to the band gap of perfect diamond at the corresponding density.

Density (g/cc)	cluster (eV)	diamond (eV)
3.5	4.1	5.4
3.7	5.0	5.6
3.9	5.4	5.9
4.1	5.1	7.4

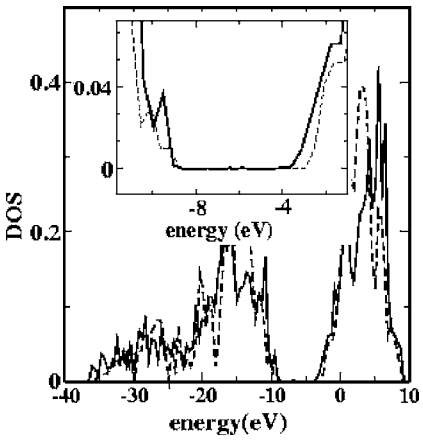

FIG. 7. Density of states of the diamond cluster at 3.9 g/cc (solid line) compared to the density of states of pure diamond (dashed line). The insert shows a magnified part of the density of states near the band gap.

In another set of simulations, three liquid samples containing 216 atoms at 3.5 g/cc and 8000 K were generated as described above with melting times of 5, 10, and 15 ps. Then each sample was compressed in one direction ($\hat{z}$) to bulk densities of 3.6, 3.7, and 3.8 g/cc and quenched to 300 K with different cooling rates [200 (slow), 500 (intermediate), and 1000 K/ps (fast)], 27 simulations in all. These densities were chosen from consideration of the computational convenience. After cooling, the samples were expanded in the $\hat{z}$ direction to restore their cubic form (at 3.5 g/cc) and finally relaxed during 25 ps.

The samples generated by these procedures contained some crystallites embedded in amorphous C. These structures were analyzed according to their content of differently coordinated atoms and by their radial and angular distribution functions. The band gap inside the crystallites was computed automatically during the simulations (in order to calculate the attractive part of the tight-binding potential, we need to calculate the electronic structure of the sample). The coordination number of each carbon atom was determined to be the number of its neighbors within a sphere of radius 1.9 Å centered on this atom. If this number is 4, then the atoms are assumed to be sp^3 coordinated, if the atoms have three neighbors within the sphere, then they are assumed to be sp^2 coordinated, etc. The ATOMIC VIZUALIZATION package AViz[28] enables the visualization of a samples from different directions with different color coding for differently coordinated atoms; therefore, sp^3- or sp^2-bonded ordered clusters can be clearly distinguished. AViz enables rotating and slicing the clusters to determine their crystalline structure. Each cluster was characterized by its radial and angular distribution function compared to those of the respective perfect crystal structure. The electronic structure of the clusters was also studied and compared to the electronic structure of the related perfect crystal.

III. RESULTS

A. Amorphous carbon compressed in all three directions

The structures obtained by the processes described above for samples compressed isotropically in all three directions at different densities and subjected to different cooling rates were found to depend on both pressure and cooling rate. For the cooling rate of 500 K/ps, ever increasing fractions of sp^3-bonded carbons were found with increasing pressure as summarized in Table I. The structures thus created were highly inhomogeneous, and even the relatively low-density samples contained large sp^3 clusters. It is worth mentioning that the percentage of the sp^3-coordinated atoms found in our samples is slightly higher than that found by Wang *et al.*,[22] in their samples generated by applying a rather similar procedure; however, they did not identify any diamond crystallites.

All sp^3 clusters in the lowest density samples (3.3 g/cc) were completely disordered. The largest sp^3 cluster found contained 36 atoms of amorphous carbon. The sp^3 clusters in the samples generated at 3.5 g/cc contained several small groups of 5–10 carbon atoms, which formed an ordered

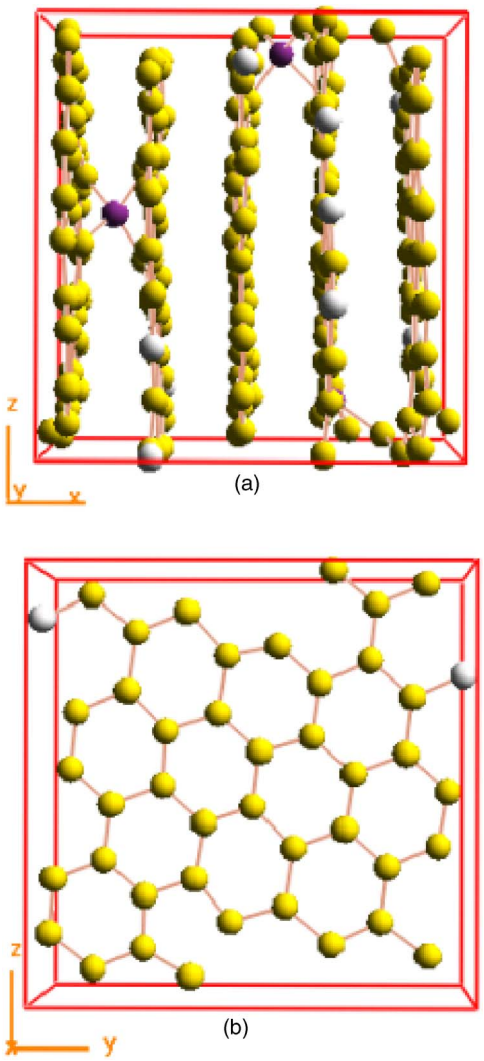

FIG. 8. (Color online) A graphitic configuration generated at 3.7 g/cc with intermediate cooling rate (a) view from the direction parallel to the graphitic planes, (b) one graphitic plane, view from the perpendicular direction. Black (purple online) balls are sp^3-coordinated atoms, gray (yellow online) balls are sp^2-coordinated atoms, and white balls are sp-coordinated atoms.

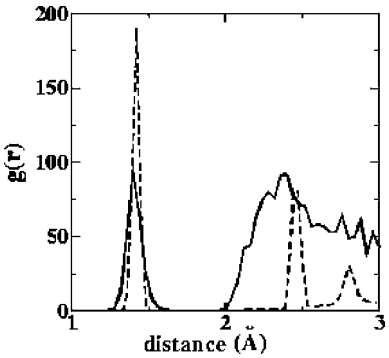

FIG. 9. Radial distribution function of the graphitic structure in the sample generated at 3.8 g/cc subjected to uniaxial pressure (solid line) compared to the radial distribution function of perfect graphite (dashed line).

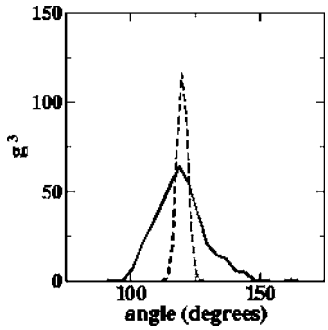

FIG. 10. Angular distribution function of the graphitic structure in the sample generated at 3.8 g/cc subjected to uniaxial pressure (solid line) compared with the angular distribution function of perfect graphite (dashed line).

structure. Each atom has four neighbors located exactly in the corners of a tetrahedron, i.e., at 109.47° and with the same bond length (1.54 Å) as in diamond (or in hexagonal diamond). These are clearly precipitates of nanodiamond.

At 3.7 g/cc, the ordered diamond clusters grew in size and contained 20–30 atoms in two cases out of five; these structures are large enough to be identified by visual inspection (using the AViz) as cubic diamond, rather than hexagonal diamond (Fig. 3). At a density of 3.9 g/cc, in four cases out of five, a nucleation of cubic diamond structures with more than 30 atoms occurred. Two very large clusters contained 90 and 120 atoms. The largest cluster of 120 atoms is shown in Fig. 4. At a density of 4.1 g/cc we found that in three cases ordered diamond crystallites containing 20–25 atoms were formed.

The orientation of the diamond clusters relative to the walls of the simulation box was found to be arbitrary. Several samples contained more than one small diamond cluster (10–15 atoms) with different orientations. In light of the above, it seems that the density of 3.9 g/cc is the most favorable density for the precipitation of diamond. The structures obtained were investigated by performing statistical analyses of their radial and angular distributions. The peak of the angular distribution function of the biggest cluster was found to be significantly narrower and higher than that of amorphous sp^3-bonded carbon (Fig. 5), indicating the high degree of order within the crystallite. The first peak of the radial distribution function (Fig. 6) is located at 1.545 Å, which is close to the bondlength of unrestricted cubic diamond, which is 1.54 Å.

The electronic structure of our samples was automatically obtained in the process of the tight-binding simulation. The band gaps in the center of the diamond clusters (before the relaxation process, i.e., at 3.9 g/cc) were found to be slightly narrower than the band gap of perfect cubic diamond at the corresponding density (see Table II and Fig. 7). The reason for this may be the influence of amorphous envelope of the clusters.

Several simulations in which the slower cooling rate (200 K/ps) was applied were performed for the samples homogeneously compressed in all three directions. Most of the samples thus generated were amorphous carbon, with all the sp^3 clusters found to be disordered. In one case for a sample with a density of 3.7 g/cc and one case for a sample with a density of 3.9 g/cc, graphitic configurations with random orientations of the graphitic planes with respect to the walls of the cell were formed as will be discussed below.

B. Amorphous carbon compressed in one direction

In order to investigate the possible formation of hexagonal diamond during the cooling of liquid carbon, the samples were subjected to the procedure described above but with the application of uniaxial pressure. The uniaxial pressure was simulated by shortening all bond components in the z direction. Samples that were prepared by applying the fast (1000 K/ps) cooling rate were found to be amorphous carbon, containing from 67 to 82 % of sp^3-coordinated atoms, depending on the pressure. The average sp^3 fraction varied from 70% for the density of 3.6 g/cc to 76% for 3.8 g/cc. These fractions are somewhat smaller than those obtained by the application of the hydrostatic pressure quoted above. All the structures were found to contain diamond clusters of different sizes and quality. No preferable orientation of the cluster relative to the direction of compression could be observed. All the clusters were identified, by careful visual inspection of the crystallites viewed from different directions, to be cubic (not hexagonal) diamond. The best quality, largest diamond cluster (~40 atoms) was generated in the sample at 3.8 g/cc. This cluster exhibits radial and angular distribution functions, which are close to those of cubic diamond. The band gap in the center of the cluster is 4.5 eV, which is somewhat smaller than that of diamond (5.4 eV).

The structures generated at intermediate (500 K/ps) and slow (200 K/ps) cooling rates fall into two groups. The first was found to contain diamond clusters embedded in an amorphous carbon network (similar to that obtained at the fast cooling rate) with a somewhat smaller fraction of sp^3. For example, for 3.7 g/cc at the slow cooling rate, an the sp^3 fraction was 66%, whereas at fast cooling rate it was 73%.

The second group of generated structures were found to be damaged graphite with interplanar distances shorter than in perfect graphite (see Fig. 8). The formation of this graphitic structure is more probable at the slow cooling rate. The orientation of the graphitic planes was found to be par-

TABLE III. Percentage of sp^3-coordinated atoms and the structure of three samples generated at different densities with applying of uniaxial pressure: the first and second at 3.8 g/cc, the third at 3.7 g/cc for different cooling rates under uniaxial pressure.

Cooling rate	Sample 1 (3.8 g/cc)	Sample 2 (3.8 g/cc)	Sample 3 (3.7 g/cc)
Fast	82% (diamond cluster)	80% (diamond cluster)	76%
Intermediate	80% (diamond cluster)	78%	Graphite
Slow	61%	Graphite	Graphite

allel to the direction of compression ($\hat{z}$) for the most cases. Only in one case (at 3.8 g/cc with the slow cooling rate) the angle between graphitic planes and the $\hat{z}$ direction was 45°. The interplanar distance varied from 2.1 Å (for the samples compressed to 3.8 g/cc) to 2.4 Å (for the samples compressed to 3.6 g/cc). The radial distribution function of the graphitic structure generated at 3.8 g/cc is drawn in Fig. 9 in comparison to the radial distribution function of perfect graphite at the same pressure. The average distance to first nearest neighbors (first peak of the radial distribution function) in the structure is shorter than that of perfect graphite (1.39 Å compared to 1.42 Å) because of the higher density of the graphitic structure. The peak of the angular distribution function (Fig. 10) is broader than in perfect graphite, but is located at 120°, as in graphite. Typical trends in our simulation can be seen in Table III, where the structures of three samples: two at 3.8 g/cc and one at 3.7 g/cc, cooled at different cooling rates are presented.

We conclude with a discussion of some particularly interesting cases that occurred in the simulations. In one of the simulations carried out at 3.7 g/cc and at slow cooling rate, the graphitic planes, after cooling, were flexed, presumably by the extreme pressure (Fig. 11). The mean bondlength in the graphitic structure was 1.41 Å, which is close to the bondlength of perfect graphite 1.42 Å. After relaxation to the density of 3.5 g/cc, at room temperature, the planes straightened out. Another interesting structure was generated at 3.8 g/cc subjected to the intermediate cooling rate. Graphite could not grow throughout the entire sample at this high density; however, the layers of the less dense graphite perpendicular to the direction of compression were found to alternate with denser diamondlike amorphous structures (Fig. 12).

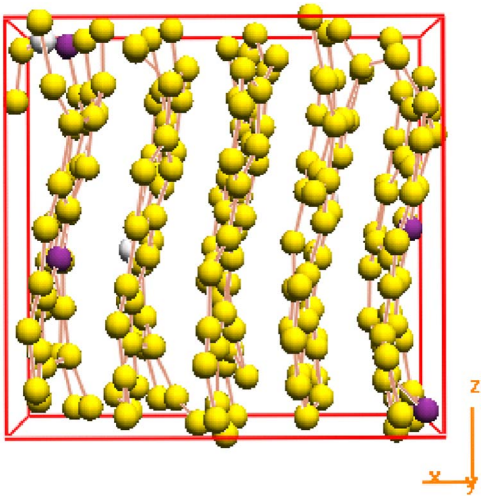

FIG. 11. (Color online) Flexed graphitic configuration generated at 3.7 g/cc with slow cooling rate. Black (purple online) balls are sp^3-coordinated atoms, gray (yellow online) balls are sp^2-coordinated atoms, and white balls are sp-coordinated atoms.

IV. DISCUSSION AND CONCLUSIONS

The conditions applied to the simulations performed here are "unrealistic" in the sense that they cannot be reached in the laboratory in any controlled way. However, similar conditions may prevail within the "thermal spike" caused by the energy transferred to the atoms of the slowing-down medium during the stopping process. The local temperatures within the volume contained in the spike (when converted to an effective temperature from the kinetic energies imparted to recoiling host atoms) may reach thousands of degrees, resulting in local melting of the material. The lifetime of this molten state is of the order of picoseconds. It is likely, though difficult to estimate qualitatively, that at the nonequilibrium conditions occuring during the thermal spike, high nonequilibrium pressures may prevail. Hence, the results obtained here may simulate those obtained during bias-enhanced nucleation, i.e., they can be compared to results obtained from experiments in which energetic carbon ions are used to create diamond nanocrystallites that serve as nucleation centers for subsequent CVD diamond growth.

Yao *et al.*[21] have observed, in high-resolution TEM studies on bias-enhanced nucleation of diamond, that well-

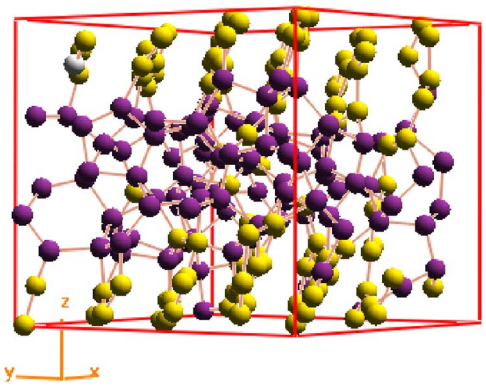

FIG. 12. (Color online) Configuration generated at 3.8 g/cc with intermediate cooling rate. Graphitic layers alternate with diamondlike amorphous carbon layers. Black (purple online) balls are sp^3-coordinated atoms, gray (yellow online) balls are sp^2-coordinated atoms, and white balls are sp-coordinated atoms.

ordered graphitic planes, oriented perpendicular to the ion-implanted surface, seem to be the precursor of the formation of nanodiamond nuclei. They proposed that some of the incoming carbon atoms are channeled between these planes. Further implantation of carbon atoms leads to the densification of the carbon phase, resulting in the formation of a dense volume of amorphous sp^3-bonded carbon atoms that eventually coalesce to form diamond nanocrystallites. These resemble the graphitic phase and diamond nucleation described in Sec. III.

The densities required to lead to the formation of graphite and diamond in our sumulation differed from those observed by Yao *et al.* However, as discussed above, this discrepancy may be attributed to the finite size effects observable in simulations of small samples.

In summary, we have simulated the formation of diamond under compression (both isotropic and uniaxial) by rapid quenching of liquid carbon with different densities and different cooling rates. The samples generated in this way were predominantly $ta-C$ amorphous carbon with ordered sp^3 clusters inside. The clusters were identified as cubic diamond. These clusters were characterized by computing the radial and angular distribution functions, which were found to be close to those of perfect cubic diamond at the same density. The band gap inside the diamond crystallites was found to be somewhat narrower than that of perfect cubic diamond. At slower cooling rates (200 K/ps), graphitic clusters were formed. It is interesting to note that the application of uniaxial pressure did not lead to the formation of lonsdaleite crystallites, but as described above, all samples appeared to be cubic diamond. However, the differences between lonsdaleite and cubic diamond are small and difficult to observe in a small crystallites.

As mentioned above, the present calculations resemble the simulations of Wang and Ho.[25,29] However, no diamond clusters were found in their work at a densities higher than 3.5 g/cc. We can see two reasons for that: first, the precipitation of diamond clusters is a random process and if the number of realizations is small, the probability of generating an amorphous carbon sample with diamond cluster inside is not large. The second reason is that it is difficult to identify a small diamond crystallite in a large amorphous sp^3-bonded carbon network without modern vizualization tools. Sometimes, in order to locate the diamond structure, the sample has to be sliced and the crystallite can be identified only from specific viewing directions. The AViz[28] (ATOMIC VIZUALIZATION package) that we used in this work possesses all the possibilities to identify the diamond clusters (rotation, slicing of the samples, color labeling of different types of atoms).

The following trends can be deduced from the present results: (i) The probability of precipitation of diamond crystallites increases with density; (ii) the probability of diamond precipitation increases as the cooling rate increases, and at slower cooling rates some samples transform to graphite; and (iii) no hexagonal diamond was found even when uniaxial pressure was applied.

These trends are in qualitative agreement with experimental results of the bias-enhanced nucleation picture[21] and also with the trends observed in detonation diamond nucleation,[13] where increasing pressure (density) and faster cooling rates leads to a higher diamond fraction in the detonation soot. In contrast, the probability of transformation to graphite increases with slower cooling rate. In the cases when the samples were compressed in one direction, the orientation of graphitic planes is parallel to the direction of compression. For the case of homogeneous compression in all three directions, the orientation of the graphitic planes obtained for the slow cooling rate is random.

ACKNOWLEDGMENTS

We are grateful to Y. Lifshitz and A. Hoffman for useful discussions. We thank A. Horsfield and M. Finnis for providing us with the OXON package.

*Electronic address: anastasy@techunix.technion.ac.il

[1] F. P. Bundy, H. T. Hall, H. M. Strong, and R. H. Wentorf, Nature (London) **176**, 51 (1955).
[2] F. P. Bundy and J. S. Kasper, J. Chem. Phys. **46**, 3437 (1967).
[3] J. E. Field, *The Properties of Diamond* (Academic Press, New York, 1979).
[4] R. M. Hazen, *The Diamond Makers* (Cambridge University Press, Cambridge, England, 1999).
[5] H. Sumiya and T. Irifune, SEI Tekunikaru Rebyu **59**, 52-9 (2005).
[6] F. P. Bundy, J. Chem. Phys. **38**, 631 (1963).
[7] A. Onodera, K. Higashi, and Y. Irie, J. Mater. Sci. **23**, 422 (1988).
[8] S. Naka, K. Horii, Y. Takeda, and T. Hanawa, Nature (London) **259**, 38 (1976).
[9] P. S. DeCarli and J. C. Jamieson, Science **133**, 1821 (1961).
[10] J. B. Donnet, E. Fousson, T. K. Wang, M. Samirant, C. Baras, and M. Pontier-Johnson, Diamond Relat. Mater. **9**, 887 (2000).
[11] N. R. Greiner, D. S. Phillips, J. D. Johnson, and F. Volk, Nature (London) **333**, 440 (1988).
[12] K. Iakoubovskii, M. V. Baidakova, B. H. Wouters, A. Stesmans, G. J. Adriaenssens, A. Ya. Vul', and P. J. Grobet, Diamond Relat. Mater. **9**, 861 (2000).
[13] V. M. Titov, V. F. Anisichkin, and I. Yu. Mal'kov, Fiz. Goreniya Vzryva **25**, 117 (1989).
[14] S. Yugo, T. Kanai, T. Kimura, and T. Muto, Appl. Phys. Lett. **58**, 1036 (1991).
[15] Y. Lifshitz, Th. Kohler, Th. Frauenheim, I. Guzmann, A. Hoffman, R. Q. Zhang, X. T. Zhou, and S. T. Lee, Science **297**, 1531 (2002).
[16] Y. Lifshitz, X. M. Meng, S. T. Lee, R. Akhveldiany, and A. Hoffman, Phys. Rev. Lett. **93**, 056101 (2004).
[17] F. Zipoli, M. Bernasconi, and R. Martonák, Eur. Phys. J. B **39**, 41 (2004).
[18] S. Scandolo, M. Bernasconi, G. L. Chiarotti, P. Focher, and E. Tosatti, Phys. Rev. Lett. **74**, 4015 (1995).

[19] Y. Tateyama, T. Ogitsu, K. Kusakabe, and S. Tsuneyuki, Phys. Rev. B **54**, 14994 (1996).
[20] S. Fahy, S. G. Louie, and M. L. Cohen, Phys. Rev. B **34**, 1191 (1986).
[21] Y. Yao, M. Y. Liao, Th. Kohler, T. Frauenheim, R. Q. Zhang, Z. G. Wang, Y. Lifshitz, and S. T. Lee, Phys. Rev. B **72**, 035402 (2005).
[22] C. Z. Wang, K. M. Ho, and C. T. Chan, Phys. Rev. Lett. **70**, 611 (1993).
[23] I. Rosenblum, J. Adler, S. Brandon, and A. Hoffman, Phys. Rev. B **62**, 2920 (2000).
[24] A. Sorkin, J. Adler, and R. Kalish, Phys. Rev. B **70**, 064110 (2004).
[25] C. Z. Wang and K. M. Ho, Phys. Rev. Lett. **71**, 1184 (1993).
[26] C. Z. Wang and K. M. Ho, J. Comput. Theor. Nanosci. **1**, 3 (2004).
[27] A. P. Horsfield, Phys. Rev. B **56**, 6594 (1997).
[28] J. Adler, A. Hashibon, N. Schreiber, A. Sorkin, S. Sorkin, and G. Wagner, Comput. Phys. Commun. **147**, 665 (2002).
[29] C. Z. Wang and K. M. Ho, Phys. Rev. B **50**, 12429 (1994).